Dot and Line Formation Analysis for Solid Inkjet Printing

Trevor J. Snyder, Xerox Corp, Wilsonville, Noel Tavan and Mark Weislogel, Portland State University, Portland, Oregon USA

Abstract

Droplet vision systems are employed to study on-drum and on-media multi-droplet line topologies in an offset solid ink printer. The experimental methods employed speak to the extensive printer characteristics that can be quantitatively studied. Several straightforward and illuminating examples are given such as drop topology as a function of dpi, line uniformity, jet precision and repeatability. A simple analytic model predicting topology is also shown. This data helps show the many benefits of an inkjet offset printing process.

Introduction

The most common printing architecture for ink jet printers is direct printing. Typically, water-based inks are used with an on-demand inkjet printhead to directly deposit ink drops on the media. In a second ink jet printing architecture, known as "offset printing" or "indirect ink jet printing" [1], the printhead images onto an intermediate transfer drum that is coated by a liquid release layer, as shown in Figure 1.

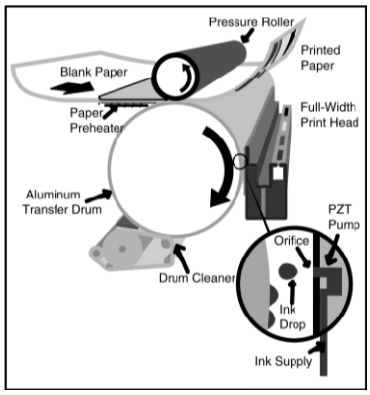

Fig 1. Offset Printing Process

Xerox employs the offset printing architecture in a family of A4 printers, MFP's, and A3 copiers. A resin-based, solid ink is loaded into the printer in its solid form. The ink is melted and dripped into a printhead. The ink flows through fluidic manifold channels and is jetted out of microscopic orifices through the use of piezoelectric transducer (PZT) technology. Jet geometries are carefully controlled and a specially designed electric pulse is applied to the PZT which together produce a precise and repeatable drop volume. The drum temperature is controlled and maintains the ink in a ductile, viscoelastic state. When the image is complete, it is transferred to the media by passing a preheated sheet between a high durometer synthetic pressure roller and the transfer drum. A high pressure is developed in the nip that compresses the paper and ink layer, spreading the ink drops, and fusing them into the media. The controlled temperature and pressure transfer process is referred to as a "transfix" or "transfuse" process. Since the entire latent image is first formed on the drum, the resulting image quality of the offset architecture is highly repeatable. This process forms a precision ink layer on the media and is relatively insensitive to media type compared to traditional inkjet and laser printers [2].

Both customers and the competitive marketplace continue to demand higher speed printers with higher resolutions, and at lower costs. To achieve these requirements, offset printer development needs to keep pace in many areas including increased transfix speeds and smaller drop masses. These requirements create the need for improved understanding of the imaging and transfix processes and the need for refined measurement tools and methods.

It is both essential and routine to evaluate and diagnose printer performance by studying the transfixed printer output. Unfortunately, the impact of the transfix process can confound printer performance by altering the 'drop-on-drum' state, which clouds the roles and relationships between the initial jetting, drop impact dynamics, solidification, and transfix. In this work, drop-on-drum and bench top vision systems are employed as tools to study single-drop and line topologies. The experimental methods employed speak to the extensive printer characteristics that can be quantitatively studied. Several straightforward and illuminating examples are given such as drop topology as a function of dpi, line uniformity, and jet precision.

Vision Systems

The vision systems in this study are composed of a Drop-On-Drum Vision System (DODVS) and Bench Top Microscope (BTM) shown in Figure 2. Both systems used identical optical paths and employed rigid frames and precision electromechanical stages to support accurate and high resolution images.

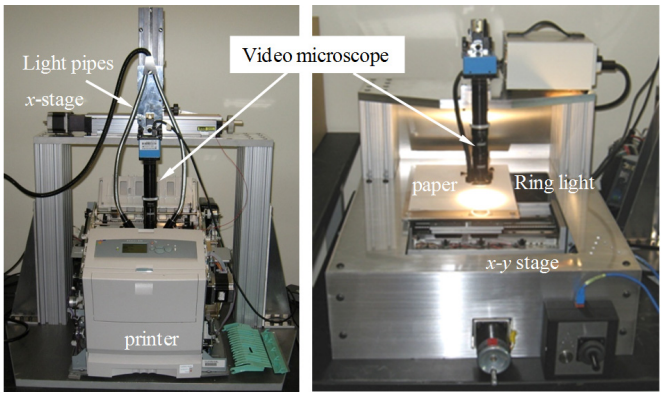

Fig 2. Vision Systems

Select images of on-drum and transfixed drops as captured by the vision systems are shown in Figure 3.

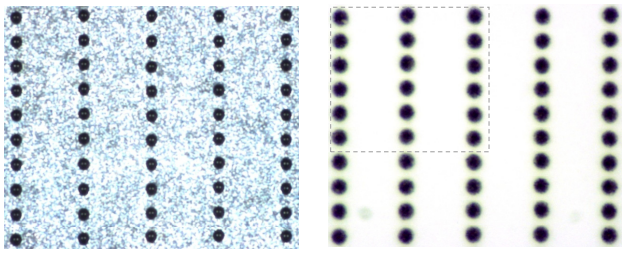

Fig. 3. Comparison of 24ng drops at 232dpi on drum (left) and media (right)

Line Quantifier Code Application

Experimental Measurements of Line Topology

Unlike liquid inkjet, solid ink droplets quickly solidify and form precise and repeatable solid structures or line topologies. Such line topologies can be classified on statistical grounds by digital processing of images such as those shown in Fig. 3. This is accomplished using a custom MATLAB® program. Each image is converted to black and white, rotated as necessary and analyzed using thresholding to identifying the boundary of each drop or drop cluster. The location of each centroid is computed as is the drop or cluster length, width, and projected area. This information is used to determine the drop topology which is separated into four categories, i.e. single, double-, triple-, and continuous lines, the latter which are herein defined as composed of more than three coalesced drops. The percent projected area of the various drop types is calculated and used as a measure of overall line topology and quality. Typical results from the line quantifier algorithm are presented in Fig. 4. In this example it is found that for 24ng drops at 436dpi, the resulting 'line' topology consists of 7% single drops, 78% double-drops, 15% triple-drops, and < 1% 'continuous lines.'

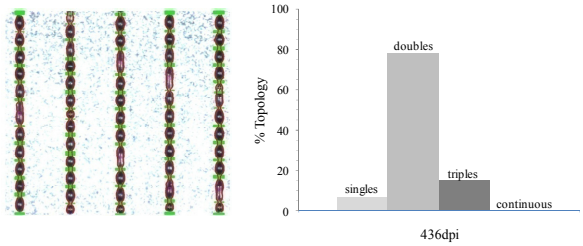

Fig. 4. Example of statistical output from the line quantifier code for 24ng drops at 436dpi

The line quantifier code can be used to efficiently and automatically map drop types. For example, a summary of statistical mixed line topologies is provided in Fig. 5 for seven different *dpi* values. Such maps can be constructed for any combination of variables: drop mass, *dpi*, drum temperature, wave function, wave amplitude, color, color combination, etc. From Fig. 5 one can accurately determine intermediate and extrapolated line topologies. One learns that:

1. Only single drop, double-drop, and continuous line topologies dominate the spectrum with triple-drops not exceeding 15% of the total.
2. The transition from single to continuous line topologies occurs for these printer conditions between 325 and 545dpi.
3. One might expect an approximately 50%-50% single-double-drop topology at approximately 385dpi and approximately a 50%-50% double-quadruple^{+}-drop topology at approximately 480dpi.
4. The double-drop topology is dominant at over 80% near 400 to 425dpi, but never achieves a 100% topology of its own.

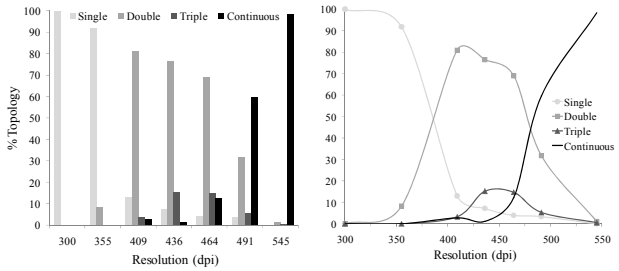

Fig. 5. Summary of drop statistics as a function of dpi for m_d = 24ng, T_D = 15.6ºC: bar chart (left) and scatter plot (right).

Jet Precision

The relative precisions of individual jets are assessed using the line quantifier code by measuring the 2-D centroid locations. Low *dpi* values (< 300dpi) were used with 24ng drops to achieve single drop lines. The average of the *x* (horizontal) and *y* (vertical) centroid variations are computed by measuring the absolute difference between the actual and ideal distance of a given drop centroid. For a given *dpi*, all differences in single drop centroids can be measured and averaged and an example data set is summarized in Fig. 6. Scatter in the *y*-direction was larger than that in the *x*-direction. In general, the small deviations in projected drop centroid for single drop lines indicate that jet/drop precision is not a primary contributor to the single to double-drop transition. However, the variations in drop centroid are suspected of contributing to some drop line topology changes.

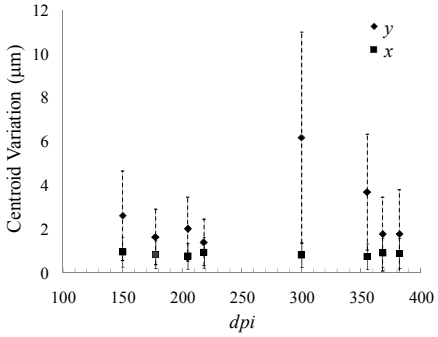

Fig. 6. Average centroid variations between nearest neighbor single drops as a function of dpi for a fixed jet with 24ng drops

Line Uniformity

The uniformity and repeatability of individual inkjets are also readily investigated by studying the line topologies at different locations on the drum for fixed *dpi* using the line quantifier code. The percentages for each line topology type for 436dpi lines (m_d

=24ng) are listed in Figure 7. In this comparison the jet-to-jet performance is relatively consistent across the drum.

Line Type % (st. dev.)	Single	Double-	Triple-	Continuous $N \geq 4$
line 15	6.4 (3.4)	86 (7.2)	9.3 (5.2)	0 (0)
20	5.7 (2.3)	78.9 (4.5)	12.2 (3.4)	3.1 (3.9)
25	4.4 (1.2)	78 (3.4)	17.6 (3.8)	0 (0)
30	6.6 (3.1)	78.1 (4.4)	13 (2.3)	2.1 (2.4)
Average	5.8 (2.3)	80.3 (5.6)	13 (4.7)	1.3 (2.5)

Fig. 7. Average centroid variations between nearest neighbor single drops as a function of dpi for a fixed jet with 24ng drops

Analytic Modeling of Line Topology

Referring to the sketch of Fig. 8, knowing the average projected drop diameter d, average drop mass m_d, and ink density ρ, by assuming capillary dominance (small Bond number, $Bo = \rho g R^2/\sigma << 1$ where g and σ are gravity and surface tension, respectively) the shape of the drop may be approximated by a spherical cap and the contact or wetting angle θ calculated from the implicit equation

$$\left(\frac{1-\cos\theta}{\sin\theta}\right)^2\left(\frac{2+\cos\theta}{\sin\theta}\right) \equiv \frac{F_s}{\sin^3\theta} = \frac{24 m_d}{\rho \pi d^3} \tag{1}$$

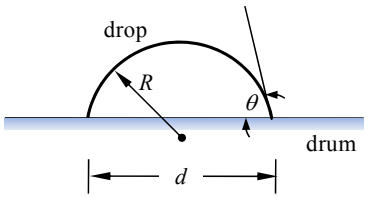

Fig. 8. Sketch of idealized Bo << 1 drop-on-drum.

Using eq. (1) and data similar to that in Fig. 3 and 4, the contact angle of black 24ng drops is found with good precision to be 40.5 ± 1.9º. The contact angle is a critical property to predict topologies for a variety of printer settings. Indeed, for a given drop mass, eq. (1) when rearranged shows that as expected the projected diameter increases with decreasing contact angle. Assuming that multi-drop lines are created as soon as two single drops first contact, and for the time being ignoring drop spreading and drawback effects during drop impact, the highest possible resolution (*dpi*) at which only single drops are present can be established. For contact angles in the range $0 \leq \theta \leq \pi/2$ (in radians), the single drop domain is approximated by

$$dpi_{single} = \frac{1}{2}\left(\frac{\pi \rho F_s}{m_d \sin^3\theta}\right)^{1/3} \tag{2}$$

For small contact angles θ << 1, eq. (2) reduces to approximately

$$dpi_{single} < \frac{1}{4}\left(\frac{2\pi\rho\theta}{m_d}\right)^{1/3} + O(\theta^{7/3}) \tag{3}$$

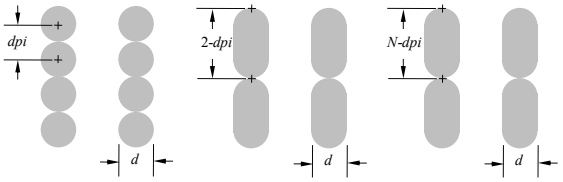

Fig. 9. Highest idealized dpi setting for single drop (left), double-drop (middle), and N-drop (right) topological profiles.

In a similar manner and as mentioned above, it is found from observations that the projected surface area of two coalesced drops, hereafter referred to as a double-drop, has the same width as a single drop, d. In this case, it is assumed that the projected 'double-drop' has a 'semi-pill-like' shape with boundaries consisting of two projected semi-circles of diameter d connected tangentially by a circular cylindrical body and with all contact lines satisfying the contact angle condition on the drum. The model is sketched in Fig. 9 (middle) and does not satisfy Laplace's equation for a capillary surface of constant curvature. Nonetheless, further support for its application will be discussed in context with Fig. 10. For $0 \leq \theta \leq \pi/2$, the model 'double-drop domain' is approximated by

$$dpi_{double} = \frac{1}{(\sin\theta + \pi F_s/3F_c)}\left(\frac{\pi\rho F_s}{m_d}\right)^{1/3} \tag{4}$$

which for $\theta << 1$ reduces to

$$dpi_{double} \approx \frac{1}{4(1+3\pi/16)}\left(\frac{2\pi\rho\theta}{m_d}\right)^{1/3} + O(\theta^{4/3}) \tag{5}$$

This approach can be continued for N-tuple-drops as sketched in Fig. 9 (right) yielding the model equation for all N with $0 \leq \theta \leq \pi/2$,

$$dpi_N = \frac{N}{2(\sin\theta + \pi(N-1)F_s/3F_c)}\left(\frac{\pi\rho F_s}{m_d}\right)^{1/3} \tag{6}$$

where $F_s \equiv (1-\cos\theta)^2(2+\cos\theta)$ is a geometric wetting function characterizing in part spherical end cap contributions, whereas $F_c \equiv 2\theta - \sin 2\theta$ is a geometric function characterizing in part cylindrical drop body contributions. For $\theta << 1$, eq. (6) reduces to

$$dpi_N \approx \frac{N}{4(1+3\pi(N-1)/16)}\left(\frac{2\pi\rho\theta}{m_d}\right)^{1/3} + O(\theta^{4/3}) \tag{7}$$

from which eqs. (3) and (5) can be confirmed for $N = 1$ and $N = 2$, respectively. Taking $N \to \infty$, eq. (6) yields the minimum *dpi* for which a continuous line is formed under such assumptions; namely,

$$dpi_{N\to\infty} \equiv dpi_{continuous} > \frac{3F_c}{2\pi F_s}\left(\frac{\pi\rho F_s}{m_d}\right)^{1/3} \tag{8}$$

which for $\theta << 1$ reduces to

$$dpi_{continuous} > \frac{4}{3\pi}\left(\frac{2\pi\rho\theta}{m_d}\right)^{1/3} + O(\theta^{4/3}) \tag{9}$$

For *dpi* values above this incipient continuous line condition, the width of 'continuous lines' is expected to grow with increasing *dpi*.

Eqs. (2)-(9) can be used to define various line topology regimes and limits as a simple function of drop mass, *dpi*, and temperature dependent properties ρ and θ. Eq. (6) is comprehensive and will be discussed shortly in connection with further presentation of experimental data.

Line Topology Results and Discussion

The experimental results of Fig. 5 are re-presented in Fig. 10 along with the analytical solutions for the various drop types using eq. (6) with N = 1, 2, 3, 4, ∞, and a contact angle of 40.5º. The experimental observations tend to agree with the analytical predictions. While this model is fairly simple in nature, corroborations with drop-on-drum images indicate that line-drop topologies may be simply estimated with knowledge of only drop properties such as *dpi*, drop mass, density and drum properties such as drum temperature and wettability (drop-drum contact angle).

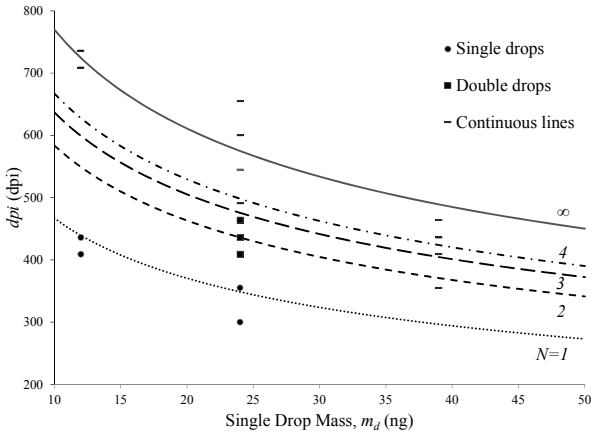

Fig. 10. Comparison of experimental (symbols) and model (lines, eq. 6) drop topologies with θ = 40.5º and ρ = 820kg/m^3.

Concerning predominately double-drop lines, the idealized critical minimum single drop spacing is determined by eq. (4) with N = 1 below which the drops first touch one another and coalesce, entering the double-drop topology. It appears the onset of the double-drop mode is reasonably predicted. From Fig. 10, for 24ng drops it appears the double-drop mode begins in earnest around 400dpi. It is interesting to note that at 382dpi the gap spacing between drops is 12μm with average jet *y*-variation error of 1.7±1.5μm. At 409dpi the gap spacing between single idealized drops is approximately 11.3μm with similar average jet *y*-variation error. Thus, the formation of the double drop mode is unlikely a result of jet accuracy and repeatability.

A more plausible explanation for the double drop phenomena is forwarded in part by Jafari and Ashgriz [5] who identify a drop merge and drawback effect. The complex but periodic double drop phenomena occurs when the maximum spread of a drop at impact causes it to collide and coalesce with the slightly oblong and potentially still molten previous drop on the drum. The most recently newly deployed drop, still molten, preferentially wets or even coalesces with the drop already on the drum and in an effort to minimize surface energy recoils in the direction of the previously deployed drop which is somewhat anchored by at least partial solidification. A larger-than-normal gap between ideal drop centroids is thus created and the next drop to be deployed lands cleanly on the drum in isolation. The process repeats. The cycle is altered at higher *dpi* eventually giving way to triple and more continuous lines.

Conclusion

Customers and competitive pressures continue to demand higher speed printers with higher quality, better reliability, and lower costs. To continue to improve offset technology and achieve these demanding customer requirements, there is a need for better understanding of the imaging and transfix processes and the need for better measurement tools and methods. In this work, drop-on-drum and bench-top vision systems are employed as tools to study the offset process in terms of drop placement and line topology. The experimental methods employed speak to the extensive printer characteristics that can be quantitatively studied.

While the results are interesting in themselves, it is hoped that the results from this work reveal how an offset solid inkjet architecture is fundamentally different compared to toner-based lasers and traditional aqueous inkjet technologies. These differences enable a truly differentiated technology able to approach the market in unique ways to satisfy the desired speed, quality, and costs. The results show that an offset latent image formation process offers excellent drop position and drop/line repeatability. Specifically, this is due to the fact that many traditional noise factors are avoided such as the basic need to even jet onto a varied media type as part of the printing process. The offset drum has an engineered surface and accurately controlled temperature. The process is also robust to image degrading physics such as aqueous ink wicking and show through, dot positional errors due to head to media spacing, paper deformation and paper cockle, and paper fiber effects on the surface of the ink and/or toner, etc.

References

[1] Snyder, T., Korol S. "Modeling the Offset Solid-Ink Printing Process," IS&T's 49th Annual Conference, 1997

[2] Snyder, T., Sheth, J., Weislogel, M., "Xerox Solid Ink Printing Technology: Media Independence Analysis", Information Management Institute, 2008

[3] Bui, L.V., Titterington, D.R., Rise, J.D., Jeager, C.W., Mutton, J, C., and Lee, H.P., Imaging process, U.S. Patent 5389958

[4] Titterington, D.R., Bui, L.V., Hirschy, L.M., Frame, H.R., Indirect printing process for applying selective phase change ink compositions to substrates, U.S. Patent 5372852

[5] Jafari, A., Ashgriz, N., Andrews, A., Drappel, S., Simulation of droplet drawback in inkjet printing, CSME 2004 Forum 1

Author Biography

This work was performed in part by M.S.M.E. student Noel Tavan. Dr. Trevor Snyder is a Principal Scientist working for Xerox in Wilsonville Oregon. Dr. Mark Weislogel is a professor at Portland State University. The latter have known each other for 20 years and collaborate on technologies which have helped in the development of numerous successful and profitable Xerox Solid Ink printers. This work was funded by a Xerox University Affairs Grant.